Onset of the sharkskin phenomenon in polymer extrusion

J. Molenaar,[1] R. J. Koopmans,[2] and C. F. J. den Doelder[2]
[1]*Mathematics Department, Eindhoven University of Technology, P.O. Box 513, 5600 MB, Eindhoven, The Netherlands*
[2]*Dow Benelux N.V., External Technologies Research and Development, P.O. Box 48, 4530 AA Terneuzen, The Netherlands*
(Received 15 October 1997)

A specific form of melt flow instabilities associated with surface defects for polymer extrudates, and commonly referred to as the ''sharkskin effect'', is modeled. When this effect occurs, a more or less regular pattern of ridges on the surface is observed resembling the skin of a shark if bent. It is shown that the relaxation oscillation model of Molenaar and Koopmans [J. Rheol. **38**, 99 (1994)] developed to describe ''spurt'' defects — in this perturbation not only the surface but the extrudate as a whole shows distortions — can be expanded to include a description for the dynamics of surface defect appearance. By introducing a nonlinear viscoelastic constitutive equation (Kaye-Bernstein-Kearsly-Zapas model) into the relaxation oscillation model a boundary layer can develop which shows oscillating behavior. Explicit criteria for the onset of this behavior are derived. The relations between these criteria and experimental parameters are pointed out. This allows for an experimental verification of the supposition that this kind of solution is the origin of the sharkskin effect. The current macroscopic approach may form the basis for the reconciliation of the debate on the origin of melt flow instabilities as either a ''slip at the wall'' or a nonmonotone ''constitutive equation'' phenomenon. [S1063-651X(98)02510-0]

PACS number(s): 83.10.Nn, 83.50.Gd, 61.41.+e

I. INTRODUCTION

Melt flow instabilities, loosely referred to as ''melt fracture,'' are phenomena limiting polymer extrusion. The occurrence of these instabilities for plastics has been known since at least 1945, as reported in Ref. [1]. Among the many papers devoted to the subject a few important reviews can be mentioned: Refs. [2], [3], and [4]. In general one distinguishes between surface and volumetric distortions of the extrudate. Considering extrusion through a capillary die, at relatively low shear flow rates, the extruded polymer strands can develop a surface with a more or less regular pattern of ridges resulting in an observable mattness or roughness. This phenomenon is often referred to as the ''sharkskin effect.'' The period of the sharkskin oscillations is typically in the order of 0.01 s. The prevalent trend in literature is to associate this sharkskin effect with material slippage at the wall due to a failure of adhesion between the solid die wall and the fluid. Various experimental findings in, for example, Refs. [5], [6], and [7] seem to support a nonzero wall velocity v_{wall}. This leads to some empirical correlations defining v_{wall} in terms of wall shear stress values (Ref. [8]) or eventually to a model proposed by [9] determining v_{wall} in terms of differences in surface tension between polymer and die material. However, not all experimental work reported in the literature supports the wall-slip idea. For example, Refs. [10] and [11] failed to find a slip value and interpret surface defects as a consequence of a cracking of the surface at the die exit. In Ref. [12], it was explained that the cracking occurs because the surface layer is accelerated from rest to the average extrusion velocity. The acceleration causes a stretching flow, inducing tensile stresses higher than the tensile strength of the melt can withstand, giving rise to the cracking phenomenon (Ref. [13]). The absence of slip can be advocated on theoretical grounds on the basis of the existence of a nonmonotonic constitutive equation. All shear rates which give a negative sloping shear-stress–shear-rate curve are unstable (Ref. [14]). It implies that for selected shear rate values more than one shear stress values are possible causing the development of a more phase system, as worked out in Ref. [15]. As the nonmonotonic nature of the constitutive equation is defined by the molecular composition of the material (see, e.g., Ref. [16]) the possibility of a surface layer development and its associated consequences can be considered real.

On a microscopic level, a shear dependent model for slippage at a polymer-solid interface was forwarded in Ref. [17]. Slippage is induced by a few polymer chains bounded to the surface which undergo a coil-stretch transition under the shear stress. This may be understood as the buildup at the wall of a layer of polymer molecules which act as molecules ''grafted'' to the wall and ''entangled'' with the bulk of the fluid. At the transition point the grafted chains disentangle, and reduce the frictional forces significantly. Experimental evidence in Ref. [18], using evanescent-wave-induced fluorescence and fringe pattern fluorescence recovery after photobleaching allowing characterization of dynamic behavior in the immediate vicinity (70 nm) of the solid surface seem to support the theory and the development of a ''pseudo-brush'' or ''mushroom'' layer.

At higher flow rates the extrudate emerges in periodic bursts, which is reflected in a pattern of pressure oscillations. The period of these oscillations is typically on the order of 10 s. The dynamics of this so-called ''spurt'' regime can be described quantitatively in terms of the theory of relaxation oscillations in terms of the macroscopic variables of pressure and flow rate, as reported in Refs. [19] and [20]. At even higher flow rates, apparently no steady laminar shear flow mode exists, and grossly distorted extrudates emerge for many polymers. All these instabilities are restricting the extrusion of polymers for practical purposes. For all practical purposes, the first sign of any type of extrudate distortion—

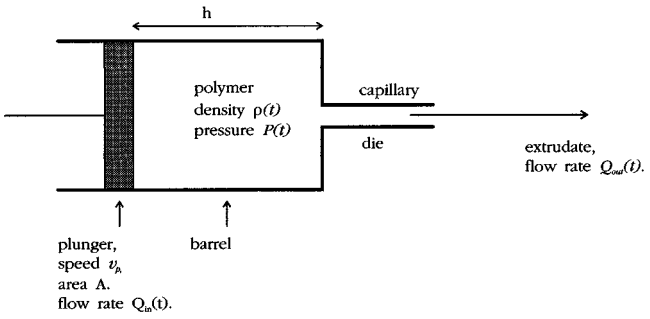

FIG. 1. Schematic drawing of the extrusion device.

often the sharkskin effect—is considered as a polymer extrusion failure. Accordingly, the capability of predicting the onset of any melt flow instability in terms of molecular composition and flow boundary conditions is critical for optimizing polymer processing.

In this paper we focus on the onset of the sharkskin instability. To that end the original one-dimensional (1D) relaxation oscillation model, proposed in Ref. [19], will be expanded into a 2D model. As for the constitutive equations use will be made of the viscoelastic model of Kaye, Bernstein, Kearsly, and Zapas (KBKZ). It is shown that the resulting model for barrel and die together admits solutions with a very thin oscillating boundary layer in the die. These surface oscillations may be appropriately interpreted as describing the sharkskin instability.

In the present approach possible slip at the wall is not included. The analysis shows that the KBKZ model also admits an oscillatory boundary layer if the no-slip condition is applied. Inclusion of slip at the wall would require a thorough and separate analysis. Since quantitative theoretical models for the slip condition in relation to extruder geometry, polymer characteristics, and velocity profile in the die are not yet available, we have to restrict the present work on this point.

An important aspect of the present model is that the onset of the sharkskin effect can be predicted in terms of the polymer properties and the extruder geometry. This enables experimental verification of the results. The present approach might also offer the possibility to rationalize both the ''wall-slip'' and ''constitutive'' origins of melt flow instabilities as valid macroscopic explanations.

The structure of this paper is as follows. The relevant conservation laws are presented in Sec. II and the resulting equations are brought into dimensionless form in Sec. III. In Sec. IV, it is shown that for low values of the pressure unique steady solutions are found, but that for pressure values above a critical one infinitely many steady solutions exist. In Sec. V the existence of solutions with an oscillating boundary layer is shown. In Sec. VI the onset of the sharkskin effect is dealt with, while in Sec. VII a discussion of the results is given.

II. MODELING THE EXTRUSION PROCESS

We consider an extrusion device, which is very simple but includes the essential elements of the extrusion process. A cross section is shown in Fig. 1. The device consists of a capillary coupled to a barrel. The polymer melt is set into motion by a plunger. Important characteristics of this system are the pressure difference P over the capillary, the volume flux Q_{out} leaving the capillary, and the volume flux Q_{in} pushed into the system by the plunger. The pressure in the barrel is assumed to be uniform. We study the extrusion device under the condition that the plunger velocity v_p is kept constant. This implies that

$$Q_{\mathrm{in}}=v_{\mathbf{p}}\,A, \tag{2.1}$$

is also constant. Here A is the area of the plunger.

The flow in the capillary has extensively been studied in Refs. [21–23]. These references showed that the flow in the capillary can be described as an axisymmetric, incompressible, shear flow. The velocity profile $v(t,r)$ in the capillary is a function of time t and the radial coordinate r only, and not of the position along the capillary. The shear rate $\omega(t,r)$ is then given by

$$\omega(t,r)=-\frac{\partial v(t,r)}{\partial r}. \tag{2.2}$$

Because of axisymmetry we have, for all t, the condition

$$\omega(t,0)=0. \tag{2.3}$$

At the wall we impose the no-slip condition

$$v(t,R)=0, \tag{2.4}$$

where R is the radius of the capillary. Using the conditions above we can write the volume flux Q_{out} through the capillary as

$$Q_{\mathrm{out}}(t)=2\pi\int_0^R v(t,r)r\;dr=\pi\int_0^R \omega(t,r)r^2\;dr. \tag{2.5}$$

The modeling of the extrusion process is based on conservation laws. In the following we shall apply the laws of conservation of mass and momentum, respectively.

A. Conservation of mass

Since the flow in the capillary is assumed to be incompressible, conservation of mass is trivially satisfied there. In the barrel the compressibility of the polymer melt has to be taken into account. Denoting the height of the barrel by $h(t)$ and the (uniform) density of the melt by $\rho(t)$, the total mass in the barrel is given by $Ah\rho$, while the mass flux leaving the barrel into the capillary is given by ρQ_{out}. Conservation of mass in the barrel is then expressed by the equation

$$\frac{d}{dt}\,(Ah\rho)=-\rho Q_{\mathrm{out}}. \tag{2.6}$$

The melt compressibility χ of the polymer is defined by

$$\frac{1}{\rho}\,\dot{\rho}=\chi\dot{P}, \tag{2.7}$$

where the notation $\dot{\rho}\equiv d\rho/dt$ is used. Using $\dot{h}=-v_p$, Eqs. (2.1), and (2.7), we may rewrite (2.6) in the form

$$\dot{P} = \frac{1}{A\chi h}\,\Delta Q, \tag{2.8}$$

with the definition $\Delta Q = Q_{\rm in} - Q_{\rm out}$. The change of h, given by v_p, is much slower than the typical period of the sharkskin phenomenon. Because of that h is assumed to be constant throughout the present analysis.

B. Conservation of momentum

The velocity profile in the capillary is determined by the following balance of linear momentum:

$$\rho\left(\frac{\partial \mathbf{v}}{\partial t} + (\mathbf{v}\cdot\boldsymbol{\nabla})\mathbf{v}\right) = \boldsymbol{\nabla}\cdot\mathbf{T}, \tag{2.9}$$

where $\mathbf{v}$ is the velocity and $\mathbf{T}$ the total, symmetric stress tensor. As usually, $\mathbf{T}$ is written as the sum

$$\mathbf{T} = -p\mathbf{I} + 2\eta\mathbf{D} + \mathbf{S}. \tag{2.10}$$

Here $\mathbf{I}$ is the unit tensor, p the pressure in the capillary, η the coefficient of the Newtonian viscosity, and $\mathbf{D}$ the rate-of-deformation tensor

$$\mathbf{D} = \tfrac{1}{2}\,(\boldsymbol{\nabla}\mathbf{v} + (\boldsymbol{\nabla}\mathbf{v})^T). \tag{2.11}$$

The form of $\mathbf{S}$ in Eq. (2.10) follows from the specific constitutive model under consideration. For this we choose the KBKZ model, which will be introduced in some detail underneath.

C. KBKZ model

The KBKZ model is a nonlinear viscoelastic model including memory effects. Full expositions of this model are given in Refs. [24, 25]. Here we use the version which is appropriate for the present system and described by Refs. [26, 21]. This version includes only one relaxation rate explicitly. This dominant relaxation rate is included into $\mathbf{S}$ in Eq. (2.10). The rest of the spectrum is represented by the term with the Newtonian viscosity η in Eq. (2.10). Details of this modeling approach are given by Ref. [27]. In view of the symmetry of the capillary we use cylindrical coordinates, with radial coordinate r and axial coordinate z. As origin we choose the point where the capillary merges into the barrel.

In the KBKZ model the pressure p in the capillary has the form

$$p(t,r,z) = P(t)\,\frac{L-z}{L} + \mu\lambda\int_{-\infty}^{t} \frac{1}{c+\gamma^2(t,\tau,r)}\,e^{-\lambda(t-\tau)}d\tau. \tag{2.12}$$

Here L is the length of the capillary, μ the elastic shear modulus, λ the relaxation rate, and c a dimensionless constant. The quantity γ is the magnitude of the shear strain at time t if the strain is applied in the past at time τ:

$$\gamma(t,\tau,r) = \int_{\tau}^{t}\omega(s,r)\,ds. \tag{2.13}$$

From Eq. (2.12) it is seen that p is the sum of an ''internal'' term including memory effects through an integral over the past, and an ''external'' term, which varies linearly along the capillary.

By Ref. [21], it is shown that the momentum equation can be written as

$$\eta\omega + \mu\,\frac{\gamma(t,0,r)}{c+\gamma^2(t,0,r)}\,e^{-\lambda t} + \mu\lambda\int_0^t \frac{\gamma(t,\tau,r)}{c+\gamma^2(t,\tau,r)}\,e^{-\lambda(t-\tau)}d\tau = \frac{1}{2}\,r\,\frac{P(t)}{L} - \frac{\rho}{r}\int_0^r \xi\,\frac{\partial v(t,\xi)}{\partial t}\,d\xi \tag{2.14}$$

for $0 \leqslant r \leqslant R$ and $t \geqslant 0$. The extrusion is assumed to have started at $t=0$.

We are interested in the behavior of the system after the transient phenomena have died out, so in the limit $t\to\infty$. The second term in the left-hand side of Eq. (2.14) can then be neglected. After the shift $t-\tau\to\tau$ in the third term of Eq. (2.14) we obtain the equation

$$\eta\omega(t,r) + \mu\lambda\int_0^t \frac{c\,\gamma(t,t-\tau,r)}{c+\gamma^2(t,t-\tau,r)}\,e^{-\lambda\tau}d\tau = \frac{1}{2}\,r\,\frac{P(t)}{L} - \frac{\rho}{r}\int_0^r \xi\,\frac{\partial v(t,\xi)}{\partial t}\,d\xi. \tag{2.15}$$

III. DIMENSIONLESS MODEL

The equations in Sec. II can be analyzed in detail only if they are put into dimensionless form. The dimensionless quantities will be denoted using the superscript *. Natural choices for the units of length and time are R and λ^{-1}, respectively. So

$$r^* = \frac{r}{R}, \quad t^* = \lambda t. \tag{3.1}$$

For the velocity, the shear rate, and the shear strain profiles, we take

$$v^* = \frac{1}{\sqrt{c}R\lambda}\,v, \quad \omega^* = \frac{1}{\sqrt{c}\lambda}\,\omega, \quad \gamma^* = \frac{1}{\sqrt{c}}\,\gamma. \tag{3.2}$$

The fluxes in Eqs. (2.1) and (2.5) are scaled accordingly:

$$Q_{\rm in}^* = \frac{1}{\sqrt{c}R^3\lambda}\,Q_{\rm in},$$

$$Q_{\rm out}^*(t^*) = \frac{1}{\sqrt{c}R^3\lambda}\,Q_{\rm out}(t) = \pi\int_0^1 \omega^*(t^*,r^*)(r^*)^2 dr^*. \tag{3.3}$$

The pressure P is scaled with the shear modulus μ:

$$P^*(t^*) = \frac{1}{\sqrt{c}\mu}\,P(t). \tag{3.4}$$

The mass conservation equation (2.8) then transforms into

$$\frac{dP^*}{dt^*} = \nu \Delta Q^*, \tag{3.5}$$

where the dimensionless quantity ν is defined by

$$\nu = \frac{R^3}{A\chi h \mu}. \tag{3.6}$$

The accumulated shear strain γ in Eq. (2.13) is already dimensionless. The KBKZ momentum equation (2.15) reads, in dimensionless form,

$$\eta\lambda\omega^*(t^*,r^*) + \mu \int_0^{t^*} \frac{\gamma^*(t^*,t^*-\tau^*,r^*)}{1+(\gamma^*(t^*,t^*-\tau^*,r^*))^2}\, e^{-\tau^*} d\tau^* = \frac{1}{2}\frac{R\mu}{L}\, r^*P^* - \frac{R^2\lambda^2\rho}{r^*} \int_0^{r^*} \xi^* \frac{\partial v^*(t^*,\xi^*)}{\partial t^*}\, d\xi^*. \tag{3.7}$$

To simplify the notation we introduce the function

$$h(x) = \frac{x}{1+x^2}, \tag{3.8}$$

with derivative

$$h'(x) = \frac{d}{dx}\, h(x) = \frac{1-x^2}{(1+x^2)^2}. \tag{3.9}$$

Dividing Eq. (3.7) by μ and using Eq. (3.8), we find

$$\varepsilon\omega^* + \int_0^{t^*} h(\gamma^*(t^*,t^*-\tau^*,r^*)) e^{-\tau^*} d\tau^* = \frac{1}{2}\beta r^*P^* - \frac{\alpha}{r^*} \int_0^{r^*} \xi^* \frac{\partial v^*(t^*,\xi^*)}{\partial t^*}\, d\xi^*, \tag{3.10}$$

with the definitions

$$\varepsilon = \frac{\eta\lambda}{\mu}, \quad \beta = \frac{R}{L}, \quad \alpha = \frac{R^2\lambda^2\rho}{\mu}. \tag{3.11}$$

The parameter ε is the ratio of the Newtonian viscosity η and the extra stress viscosity μ/λ. Note that the quotient α/ε is the Reynolds number $R^2\lambda\rho/\eta$. For the materials under consideration we have that $\alpha \ll 1$. The last term in Eq. (3.10) will therefore be neglected in the following. In practice we also have $\varepsilon \ll 1$. However, the term with ε cannot be omitted. The product $\varepsilon\omega^*$ will be shown to play an important role in the model.

The analysis in the next sections is based on the dimensionless equations. Because confusion is hardly possible, the * symbol will be omitted.

IV. STEADY SOLUTIONS

If the operating conditions are kept constant, the extrusion process is experimentally observed to converge to a constant or periodic solution when time proceeds. Here we analyze whether the model presented in Sec. III admits constant solutions, thus with the ω and v profiles being independent of time. If ω does not depend on t, we have, from Eq. (2.13),

$$\gamma(r,t,\tau) = \omega(r)(t-\tau). \tag{4.1}$$

Substitution of this into Eq. (3.10) yields the KBKZ momentum equation

$$H(\omega(r)) = \tfrac{1}{2}\,\beta r P, \quad 0 \leqslant r \leqslant 1, \tag{4.2}$$

with

$$H(\omega) = \varepsilon\omega + \int_0^{\infty} h(\omega\tau) e^{-\tau} d\tau. \tag{4.3}$$

Here we have taken the limit $t \to \infty$.

For $\varepsilon \ll 1$, H is a nonmonotonic function of ω as shown in Fig. 2. The curve has a relative maximum $H_{\max}$ at $\omega_{\max}$, and a relative minimum $H_{\min}$ at $\omega_{\min}$. From Fig. 2 it is immediately seen that Eq. (4.2) has a unique solution only if the right-hand side attains a value smaller than $H_{\min}$. For values of the right-hand side in the range $(H_{\min}, H_{\max})$, the equation has three solutions. In Table I, values for $\omega_{\max}$, $H_{\max}$, $\omega_{\min}$, $H_{\min}$, and $\bar{\omega}_{\min}$ are given.

V. OSCILLATING BOUNDARY LAYERS

The sharkskin effect is typically a boundary layer effect: the surface of the extrudate shows the sharkskin pattern, whereas the inner core of the extrudate does not show any sign of oscillating behavior. Here we analyze whether the observed phenomena can be described in terms of the models presented above. Our purpose is to show that the nonmonotonicity of the stress-strain relation implies that the flow in

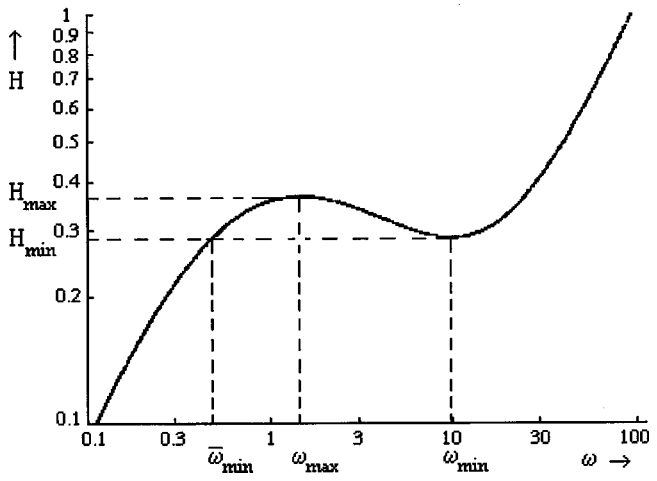

FIG. 2. The function H in Eq. (4.3) for $\varepsilon = 0.01$.

TABLE I. Values of the quantities denoted in Fig. 2 for various values of ε.

ε	$\omega_{\max}$	$H_{\max}$	$\omega_{\min}$	$H_{\min}$	$\overline{\omega}_{\min}$
0.001	1.32	0.35	48.7	0.12	0.13
0.003	1.34	0.35	23.9	0.18	0.23
0.010	1.46	0.36	10.0	0.29	0.48
0.025	1.96	0.39	3.91	0.38	1.37

the capillary may develop an oscillating boundary layer, which might be related to the observed sharkskin effect.

For higher values of the pressure, i.e., if $\frac{1}{2}\beta P > H_{\min}$, the momentum equations (4.2) have infinitely many constant solutions, due to the nonmonotonicity of the function H as shown in Fig. 2. Here we shall investigate whether Eqs. (4.2) have solutions which are oscillating near the wall and constant elsewhere in the capillary. Because the sharkskin oscillations have small amplitudes, we shall investigate small amplitude perturbations of constant solutions. In view of the fact that observed oscillations are localized near the wall, we search for solutions that are constant everywhere except for a very thin boundary layer of thickness δ.

The extrusion device is assumed to operate in the constant flux mode, so with Q_{in} being constant. Let us denote an arbitrary constant solution of the momentum equations corresponding to the (constant) pressure P_0 by $\omega_0(r)$. In a constant state we have $Q_{\text{out}}=Q_{\text{in}}$. A solution oscillating around this constant solution can be written as

$$\omega(t,r)=\omega_0(r)+\omega_1(r)e^{i\vartheta t}, \tag{5.1a}$$

$$Q_{\text{out}}(t)=Q_{\text{in}}+Q_1 e^{i(\vartheta t+\varphi_1)}, \tag{5.1b}$$

$$P(t)=P_0+2\delta P_1 e^{i(\vartheta t+\varphi_2)}, \tag{5.1c}$$

where $\vartheta \geqslant 0$ is the angular frequency of the oscillation, and φ_1 and φ_2 are possible phase differences.

The factor 2δ in Eq. (5.1c) is introduced to model the coupling between the die and the barrel in a consistent way. In the die we expect a pressure oscillation of amplitude P_1 only in the boundary layer, while the inner layer is not perturbed. Effectively we thus have $P_1=0$ in the inner layer. The pressure P in the barrel is taken to be uniform. The contribution of the pressure oscillations P_1 in the die to P is therefore weighted as follows. The die and the barrel are in contact via a cross section of the die with area π in nondimensional units. Of this area $2\pi\delta$ belongs to the boundary layer and the rest to the inner layer. The ratio of these areas is taken as weighting factor.

The amplitudes ω_1, Q_1, and P_1 of the perturbations are assumed to be small with respect to ω_0, Q_{in}, and P_0, respectively. Because of this we may linearize the momentum equations around the constant state.

The phase differences φ_1 and φ_2 are easily found. Substituting (5.1a) into (3.3b) we obtain

$$Q_{\text{out}}(t)=\pi\int_0^1 \omega_0(r)r^2dr+\pi e^{i\vartheta}\int_0^1 \omega_1(r)r^2dr. \tag{5.2}$$

Comparing this with Eq. (5.1b) we conclude from the fact that Q_1 is real that

$$Q_{\text{in}}=\pi\int_0^1 \omega_0(r)r^2dr,$$

$$Q_1=\pi\int_0^1 \omega_1(r)r^2dr,$$

$$\varphi_1=0. \tag{5.3}$$

The phase difference φ_2 follows from the mass conservation equation (3.5). Substitution of Eqs. (5.1a) and (5.1b) into Eq. (3.5) yields

$$2i\delta\vartheta P_1 e^{i\varphi_2}=-\nu Q_1. \tag{5.4}$$

Because δ, ϑ, P_1, ν, and Q_1 are real and positive, we conclude that

$$\varphi_2=\frac{\pi}{2}. \tag{5.5}$$

In Sec. VI we investigate whether the KBKZ momentum equation admits solutions which locally oscillate.

VI. KBKZ MODEL

Here we study solutions of the KBKZ equation (3.10). The nonlinearity of Eq. (3.10) comes from the integral

$$\int_0^t h(\gamma(r,t,t-\tau))e^{-\tau}d\tau, \tag{6.1}$$

with

$$\gamma(r,t,t-\tau)=\int_{t-\tau}^t \omega(s,r)ds. \tag{6.2}$$

Using representation (5.1a), we can evaluate this integral explicitly. We then obtain

$$\gamma(r,t,t-\tau)=\omega_0(r)\tau+\omega_1(r)f(\vartheta,\tau)e^{i\vartheta t}, \tag{6.3}$$

with

$$f(\vartheta,\tau)=-i\,\frac{1-e^{-i\vartheta\tau}}{\vartheta}. \tag{6.4}$$

We note that $|f(\vartheta,\tau)|\sim 1/\vartheta$ if $\vartheta\to\infty$, and $|f(\vartheta,\tau)|\sim\tau$ if $\vartheta\to 0$. The second term at the right-hand side of Eq. (6.3) is small compared to the first term. This allows for the linearization

$$h(\gamma(r,t,t-\tau))=h(\omega_0\tau)+\omega_1 f(\vartheta,\tau)e^{i\vartheta t}h'(\omega_0\tau), \tag{6.5}$$

with h' given by (3.9). Substituting (5.1a) and the linearization equation (6.5) into Eq. (3.10), we obtain the sum of the unperturbed part, satisfying Eq. (4.2), and the perturbed part, given by

$$\omega_1(r)\left[\varepsilon+\int_0^\infty f(\vartheta,\tau)h'(\omega_0(r)\tau)e^{-\tau}d\tau\right]=\frac{1}{2}\,i\beta r P_1. \tag{6.6}$$

Writing the factor $f(\vartheta,\tau)$ in the form

$$f(\vartheta,\tau)=\frac{1}{\vartheta}\,[\sin(\vartheta\tau)+i(\cos(\vartheta\tau)-1)], \tag{6.7}$$

we can split Eq. (6.6) into its real and imaginary parts. This yields the equations

$$\omega_1(r)[\varepsilon\vartheta-g_1(\omega_0(r),\vartheta)]=0 \tag{6.8}$$

and

$$\omega_1(r)g_2(\omega_0(r),\vartheta)=\tfrac{1}{2}\,\beta\vartheta r P_1, \tag{6.9}$$

where the functions g_1 and g_2 are defined as

$$g_1(\omega_0,\vartheta)=-\int_0^\infty h'(\omega_0\tau)\sin(\vartheta\tau)e^{-\tau}d\tau \tag{6.10}$$

and

$$g_2(\omega_0,\vartheta)=\int_0^\infty h'(\omega_0\tau)(\cos\,\vartheta\tau-1)e^{-\tau}d\tau. \tag{6.11}$$

Because the perturbations are nonvanishing in the boundary layer only, Eqs. (6.8) and (6.9) hold for $1-\delta\leqslant r\leqslant 1$. Equation (6.8) has the trivial solution $\omega_1(r)\equiv 0$, which corresponds to constant momentum. Also a nontrivial solution exists, corresponding to a periodic perturbation, provided that the equation

$$\varepsilon\vartheta-g_1(\omega_0(r),\vartheta)=0 \tag{6.12}$$

is satisfied for some $\vartheta>0$. Because it is physically unacceptable that the frequency would depend on position, we conclude that in the oscillating layer ω_0 has to be constant within the accuracy of the approximations we have made in the derivations. This implies that the boundary layer must be fairly thin; thus $\delta\ll 1$. This is in accordance with the fact that we are dealing with the onset of sharkskin. The next considerations are valid only in the limit $\delta\to 0$. In view of this we may take the factor g_2 in Eq. (6.9) to be independent of r and evaluate ω_0 always at the wall, denoting its value by

$$\omega_0(1)=\omega_{\text{wall}}. \tag{6.13}$$

In Fig. 3, $g_1(\omega_{\text{wall}},\vartheta)$ is plotted as a function of ϑ for several values of ω_{wall}. From this figure it is seen that Eq. (6.12) has a solution only if the slope of $g_1(\omega_{\text{wall}},\vartheta)$ at the origin is positive and steeper than the slope of the line $\varepsilon\vartheta$. This leads to the condition

$$\frac{\partial}{\partial\vartheta}\,g_1(\omega_{\text{wall}},\vartheta)\big|_{\vartheta=0}=-\int_0^\infty h'(\omega_{\text{wall}}\tau)\tau e^{-\tau}d\tau>\varepsilon. \tag{6.14}$$

From Eq. (4.3) we find that condition (6.14) is equivalent to the condition

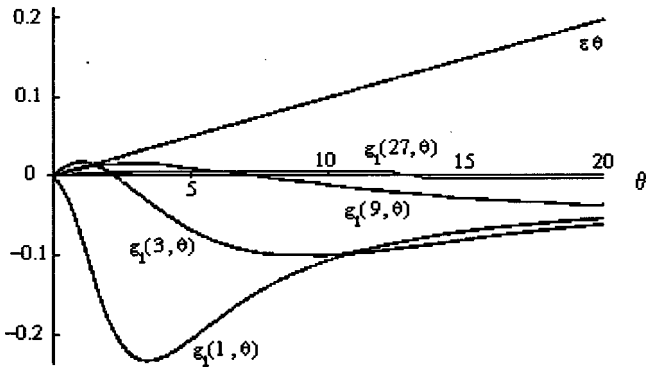

FIG. 3. The function g_1 as a function of ϑ for $\omega_{\text{wall}}=1$, 3, 9, and 27. Also, the function $\varepsilon\vartheta$ is drawn for $\varepsilon=0.01$.

$$\frac{d}{d\omega}\,H(\omega)<0. \tag{6.15}$$

This implies that Eq. (6.12) has a solution only if ω_{wall} lies in the range where H has negative slope. Also refer to Fig. 2, where H is drawn for $\varepsilon=0.01$. Conditions (6.14) and (6.15) thus imply $\omega_{\max}<\omega_{\text{wall}}<\omega_{\min}$, as indicated in Fig. 4. The resulting $\omega_0(r)$ profile has thus a discontinuity as shown in Fig. 5. The corresponding velocity profile, obtained by integrating the ω_0 profile, has a discontinuity in the slope at $r=1-\delta$ as shown in Fig. 6. It remains to analyze Eq. (6.9). Multiplying both sides of Eq. (6.9) by πr^2 and integrating over the boundary layer $1-\delta\leqslant r\leqslant 1$, we obtain

$$Q_1 g_2(\omega_{\text{wall}},\theta)=\frac{\pi}{2}\,\beta\theta\delta P_1. \tag{6.16}$$

Combining Eqs. (5.4) and (6.16), we may eliminate Q_1 and P_1. This yields

$$g_2(\omega_{\text{wall}},\theta)=\frac{\pi}{4}\,\beta\nu. \tag{6.17}$$

The present model predicts that sharkskin may occur if both conditions (6.15) and (6.17) are satisfied. Condition (6.15) implies that $\omega_{\text{wall}}\in[\omega_{\max},\omega_{\min}]$ should hold with $\omega_{\max}$ and

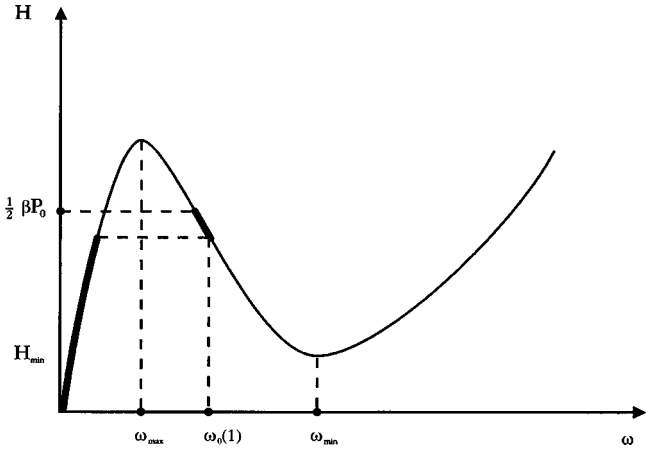

FIG. 4. The thick line indicates a possible shear rate profile satisfying Eq. (4.2). The position of the jump from the left branch to the middle branch determines the thickness of the boundary layer.

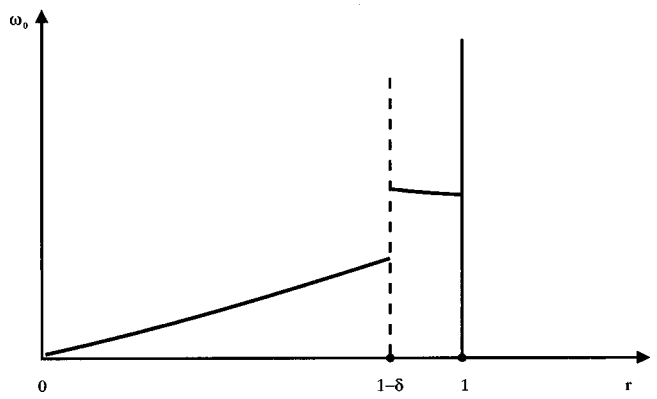

FIG. 5. The shear rate profile corresponding to the construction in Fig. 4. Here δ is the thickness of the boundary layer.

$\omega_{\min}$ to be read from Table I. These values depend on ε. Condition (6.17) further restricts the number of possible solutions. We have numerically determined the pairs $(\omega_{\text{wall}}, \beta\nu)$ with $\omega_{\text{wall}} \in [\omega_{\max}, \omega_{\min}]$, such that Eq. (6.17) has a solution for positive ϑ. The results are summarized in Fig. 7 for various values of ε. The contour lines in this figure represent the solutions of Eq. (6.17) with ϑ real and positive. The points off these lines correspond to solutions with complex ϑ. Inside the contour lines the imaginary part of ϑ is positive, outside the contour lines it is negative.

In Fig. 7, two regions can be clearly discerned. For $\varepsilon < 0.025$ two values for ω_{wall} are found as long as $\beta\nu < 0.01$. These values are quite close to $\omega_{\max}$ and $\omega_{\min}$. On the other hand, for $\beta\nu > 0.05$ no solution exists, and this holds for all ε.

We note that in the limit $\beta\nu \to 0$ the contour lines approach the values of $\omega_{\min}$ and $\omega_{\max}$. Following Eq. (3.5), this limiting case corresponds to the system being held under constant pressure. From Eq. (5.4) we conclude that $P_1 = 0$ if $\nu = 0$, so in that case an oscillating boundary layer does not exist.

VII. ONSET OF THE SHARKSKIN EFFECT

A central issue in any theory about polymer flow instabilities is the question whether a critical value Q_{crit} exists

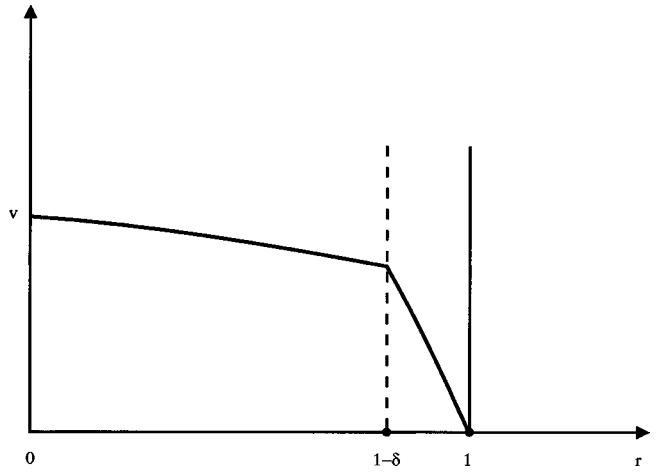

FIG. 6. The velocity profile corresponding to the shear rate profile in Fig. 5.

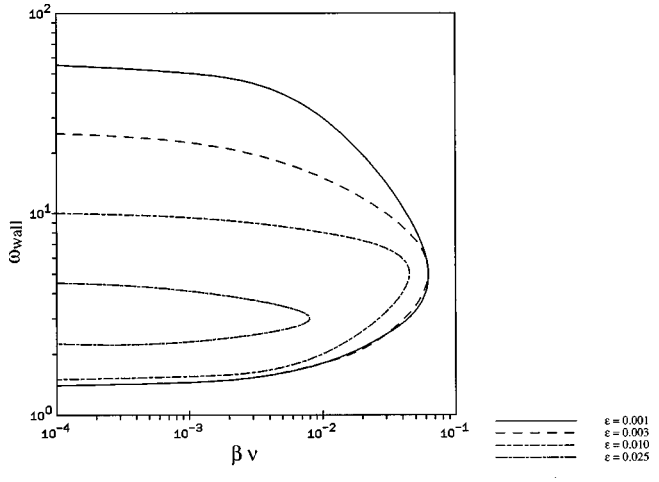

FIG. 7. Contour lines indicating the solutions of Eq. (6.17) in the $(\beta\nu, \omega_{\text{wall}})$ plane.

such that the instability does not occur for $Q_{\text{in}} < Q_{\text{crit}}$, but may occur for $Q_{\text{in}} \geqslant Q_{\text{crit}}$. Of course, not only is the existence of such a transition of importance, but also the possibility to calculate its value in terms of the polymer properties and the extruder geometry. We shall point out here the consequences of the analysis in Sec. V for Q_{crit}. Because we have already seen that the essential dimensionless parameters are ε and the product $\beta\nu$, we show how to find Q_{crit} as a function of these two parameters.

Condition (6.15) states that ω_{wall} must lie on the second branch of H, where this function has negative slope; see Fig. 2. Condition (6.17) further restricts the number of ω_{wall} values for which the sharkskin effect may occur. From the contour plot in Fig. 7 we find that two values for ω_{wall} are found if $\beta\nu$ is small enough. In Fig. 8 these values are indicated as ω_a and ω_b, with $\omega_{\max} \leqslant \omega_a \leqslant \omega_b \leqslant \omega_{\min}$. For small values of Q_{in} the pressure P is small. From Eq. (4.2) and Fig. 2, it then follows that the $\omega(r)$ profile is completely situated on the left branch of H.

Let us follow what happens if, as is usual in the experiments, Q_{in} is increased so gradually that, apart from transient phenomena, Eq. (4.3) remains valid. We focus now on the regime in which the system does not yet show volumetric distortions. Then, $Q_{\text{out}} \sim Q_{\text{in}}$. We wonder when surface distortions, thus the sharkskin effect, may appear for the first time.

An increase of Q_{in} implies an increase of the pressure P, and thus of H, and thus of ω_{wall}. In Fig. 2, we observe that ω_{wall} can attain a value on the second branch if H passes the value $H_{\min}$, and ω_{wall} thus passes the value $\overline{\omega}_{\min}$.

From Fig. 8 we see that the sharkskin effect may occur if H attains the value $H(\omega_b)$ for the first time. We thus conclude that the possible onset of the sharkskin effect is determined by the condition $\omega_{\text{wall}} = \overline{\omega}_b$. The corresponding $\omega(r)$ profile is completely situated on the left branch of H between 0 and $\overline{\omega}_b$. The corresponding critical value Q_{crit} can be calculated from Eq. (3.3b).

In Fig. 9 we have drawn Q_{crit} as a function of $\beta\nu$ for $\varepsilon = 0.01$. For other ε values the results are quite similar. We discern the same two regimes as found in Fig. 7: Q_{crit} is nearly independent of $\beta\nu$ if $\beta\nu < 0.02$, whereas for larger values, $\beta\nu > 0.05$ say, no sharkskin effect can occur, i.e.,

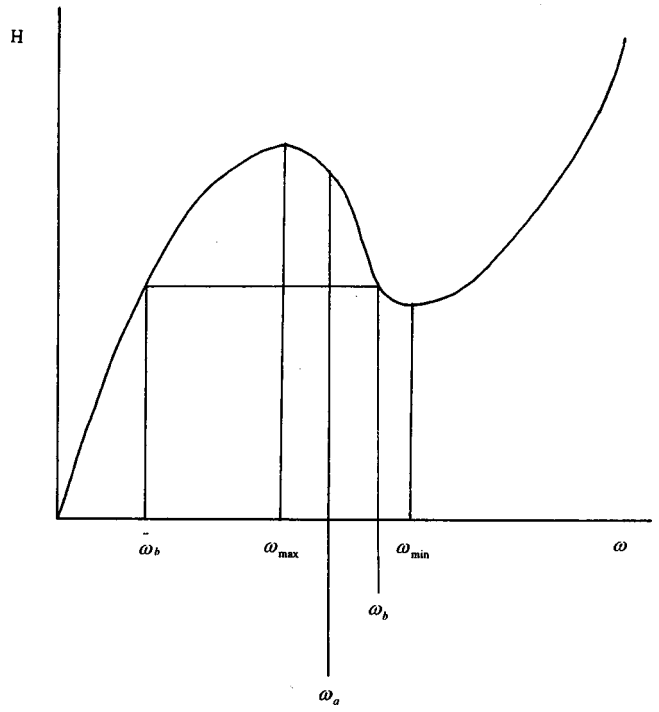

FIG. 8. Position of ω_a and ω_b in the (ω,H) plane.

$Q_{crit}=\infty$. So we conclude that, in a good approximation, Q_{crit} only depends on ε as long as $\beta\nu$ is small. This dependence is given in Fig. 10. Note that Q_{crit} is a dimensionless quantity; the dimensionful value is obtained from the scaling in Eq. (3.3). Another interesting feature of the model is that it predicts the angular frequency of the sharkskin oscillations. In Fig. 11 the value of the dimensionless frequency ϑ is given as a function of $\beta\nu$ for $\varepsilon=0.01$. The dimensionful frequency is found from the scaling in Eq. (3.1). In Fig. 11 it is seen that $\vartheta\to 0$ if $\beta\nu\to 0$. Above we have found that for $\beta\nu > 0.05$ the sharkskin effect does not occur. From Fig. 11 we find that for very small $\beta\nu$ values the sharkskin effect may occur but with such a low frequency that it will not be detected experimentally.

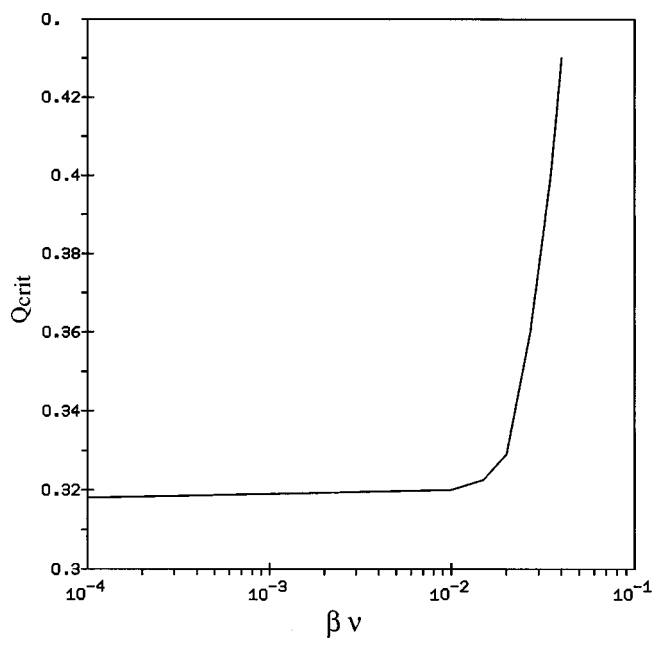

FIG. 9. Q_{crit} as a function of $\beta\nu$ for $\varepsilon=0.01$.

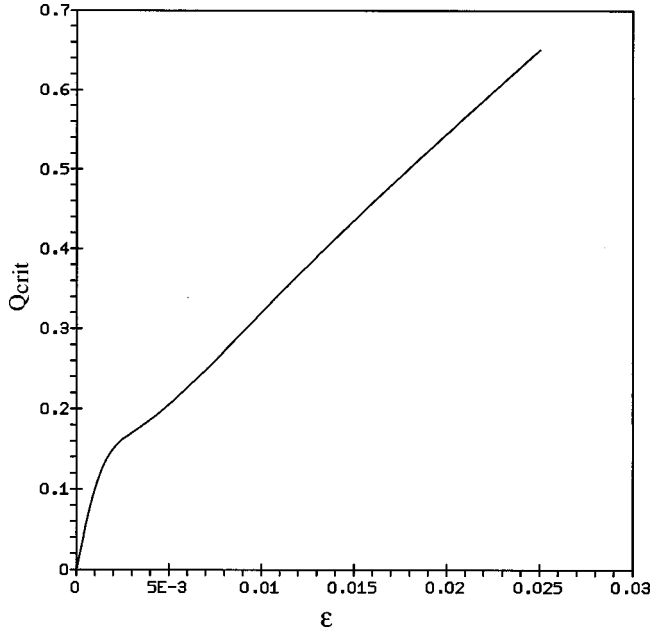

FIG. 10. Q_{crit} as a function of ε.

VIII. DISCUSSION

In Secs. V and VI, we have shown that the model in Sec. II, describing polymer shear flow through a die coupled to a barrel, admits solutions with a thin, oscillating boundary layer in the die. As constitutive equation the KBKZ model has been used. However, in Ref. [28] it was shown that application of the Johnson-Segalman-Oldroyd model (see Refs. [24, 25]) leads to very similar results, although the formulas involved are quite different from the KBKZ expressions above.

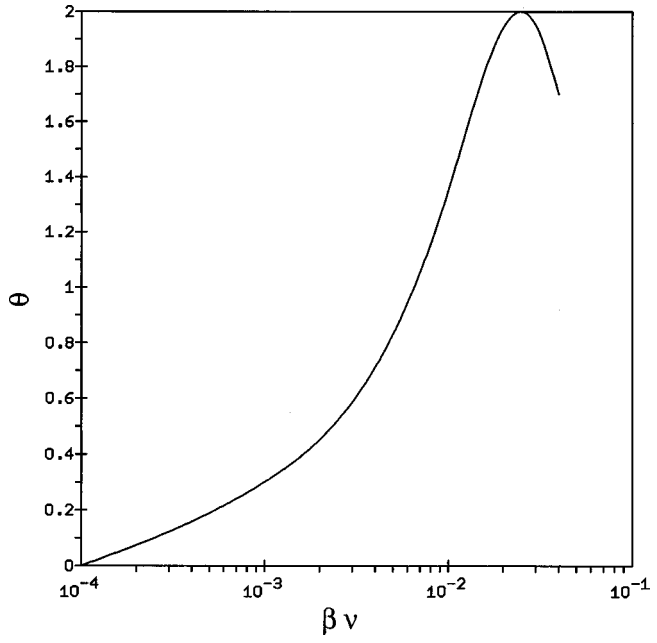

FIG. 11. Angular frequency ϑ as a function of $\beta\nu$ for $\varepsilon=0.01$.

The existence of oscillating solutions depends on the dimensionless parameters ε and $\beta\nu$, introduced in Eqs. (3.6) and (3.11). These parameters are determined by the characteristics of both the extruder geometry and the polymer properties. It is found that an oscillating boundary layer exists only if $\beta\nu$ is small enough. As a rule of thumb we formulate this as the condition

$$\beta\nu \equiv \frac{R^4}{A\chi h\mu L} < 0.05. \tag{8.1}$$

If Eq. (8.1) is fulfilled, the critical value Q_{crit} of the volume flux Q_{in} is nearly only dependent on ε, and given in Fig. 10. The angular frequencies of the oscillations do depend on $\beta\nu$, as is shown in Fig. 11.

An attractive and important feature of these results is that they allow a direct comparison with experiment. Although it might be hard to use polymers characterized by one relaxation time only, the qualitative aspects of this analysis must hold quite generally. For example, the existence of a critical value for $\beta\nu$, given in Eq. (8.1) can be quite easily checked experimentally. Because $\beta\nu$ is very sensitive to the value of the die radius R, the latter geometrical parameter is quite appropriate to be varied in the experiment. When R is varied in the experiment, not only condition (8.1) could be checked, but also the dependence of the angular frequency ϑ on $\beta\nu$, and thus on R, as predicted by the results in Fig. 11. In practice, the extrudate seldom shows a highly regular pattern of ridges. This is in accord with the analysis above, that the sharkskin effect can be interpreted as a boundary layer that becomes unstable. The possible oscillations only start if the layer is perturbed, and this will usually happen in an uncontrolled way. However, in most cases it is still possible to detect a definite frequency in the sharkskin pattern.

Another observation is that $\beta\nu \sim h^{-1}$, with h the length of the barrel. This implies that the sharkskin instability should stop, if $h \to 0$, i.e., if the barrel becomes empty, because then condition (8.1) is violated.

The critical volume flux Q_{crit} only depends on ε, and the dependence is given in Fig. 10. Because $\varepsilon = \eta\lambda/\mu$, this critical value only depends on the polymer properties. The present model predicts that the smaller ε is, the smaller Q_{crit} will be. The model further states that the dimensionful Q_{crit} scales with R^3 [cf. Eq. (3.3)]. These tendencies can easily be checked in experiments.

If the results of the present analysis qualitatively agree with the experimental data, the model can be considered as a first step in the direction of a theoretical description of extrusion instabilities. A very interesting extension would be the coupling of the present model to a model describing possible slip at the wall. An other refinement would be the inclusion of a spectrum of relaxation times. Since along these lines the relations between experimentally accessible quantities like Q_{crit} and ϑ and the geometrical and polymer melt parameters become known, this approach could be used to find extruder-polymer combinations with high values of Q_{crit} [29–31].

[1] H. K. Nason, J. Appl. Phys. **16**, 338 (1945).
[2] J. P. Tordella, in *Rheology: Unstable Flow in Molten Polymers*, edited by F. R. Eirich (Academic, New York, 1969).
[3] C. J. S. Petrie and M. M. Denn, AIChE. J. **22**, 209 (1976).
[4] R. G. Larson, Rheol. Acta **31**, 213 (1992).
[5] A. V. Ramamurthy, J. Rheol. **30**, 337 (1986).
[6] D. S. Kalika and M. M. Denn, J. Rheol. **31**, 815 (1987).
[7] S. G. Hatzikiriakos and J. M. Dealy, J. Rheol. **35**, 497 (1991).
[8] S. G. Hatzikiriakos and J. M. Dealy, J. Rheol. **36**, 703 (1992).
[9] C. W. Steward, J. Rheol. **37**, 499 (1993).
[10] J. J. Benbow and E. R. Howells, Trans. Plast. Inst. **30**, 246 (1960).
[11] J. M. Piau, N. El Kissi, F. Toussaint, and A. Mezghani, Rheol. Acta **34**, 40 (1995).
[12] F. N. Cogswell, J. Non-Newtonian Fluid Mech. **2**, 37 (1977).
[13] N. Bergem, in *Proceedings of the VII International Congress on Rheology, Goeteborg, 1976* (Central Institute for Industrial Research, Oslo, 1976), p. 23.
[14] J. R. A. Pearson, in *Proceedings of the VII International Congress on Rheology, Goeteborg, 1976* (Ref. [13]), pp. 163-181.
[15] J. K. Hunter and M. Slemrod, Phys. Fluids **26**, 2345 (1983).
[16] T. W. Huseby, Trans. Soc. Rheol. **10**, 181 (1966).
[17] F. Brochard and P. G. de Gennes, Langmuir **8**, 3033 (1992).
[18] K. B. Migler, H. Hervet, and L. Leger, Phys. Rev. Lett. **70**, 287 (1993).
[19] J. Molenaar and R. J. Koopmans, J. Rheol. **38**, 99 (1994).
[20] V. Durand, B. Vergnes, J. F. Agassant, E. Benoit, and R. J. Koopmans, J. Rheol. **40**, 383 (1996).
[21] A. C. T. Aarts and A. A. F. van de Ven, J. Eng. Math. **29**, 371 (1995).
[22] D. S. Malkus, J. A. Nohel, and B. J. Plohr, SIAM (Soc. Ind. Appl. Math.) J. Appl. Math. **51**, 899 (1991).
[23] D. S. Malkus, J. A. Nohel, and B. J. Plohr, J. Comput. Phys. **87**, 464 (1990).
[24] R. B. Bird, R. C. Armstrong, and O. Hassager, *Dynamics of Polymeric Liquids* (Wiley, New York, 1987), Vol. 1.
[25] R. I. Tanner, *Engineering Rheology* (Clarendon, Oxford, 1988).
[26] M. J. H. B. Grob, Master's thesis, Eindhoven University of Technology, 1994.
[27] R. den Adel, Master's thesis, Faculty of Mathematics and Computing Science, Eindhoven University of Technology, The Netherlands, 1996.
[28] C. F. J. den Doelder, Master's thesis, Eindhoven University of Technology, 1996.
[29] G. C. Georgiou and M. J. Crochet, J. Rheol. **38**, 639 (1994).
[30] G. C. Georgiou and M. J. Crochet, J. Rheol. **38**, 1745 (1994).
[31] M. Greenberg and Y. Demay, Eur. J. Appl. Math. **5**, 337 (1994).